Annales
Geophysicae
Discussions
Open Access

The time derivative of the geomagnetic field has a short memory

Mirjam Kellinsalmi[1,2], Ari Viljanen[1], Liisa Juusola[1], and Sebastian Käki[1,2]

[1]Finnish Meteorological Institute
[2]University of Helsinki

Correspondence: Mirjam Kellinsalmi (mirjam.kellinsalmi@fmi.fi)

Abstract.

Solar eruptions and other types of space weather effects can pose a hazard to the Earth's power grids via *geomagnetically induced currents* (GIC). In worst cases, they can even cause large scale power outages. GIC are a complex phenomenon, closely related to the time derivative of the geomagnetic field. However, the behavior of the time derivative is chaotic and has proven to be tricky to predict. In our study, we look at the dynamics of the geomagnetic field during active space weather. We try to characterize the magnetic field behavior, to better understand the drivers behind strong GIC events. We use geomagnetic data from the IMAGE (International Monitor for Auroral Geomagnetic Effect) magnetometer network between 1996 and 2018. The measured geomagnetic field is primarily produced by currents in the ionosphere and magnetosphere and secondarily by currents in the conducting ground. We use the so called *separated magnetic field* in our analysis. The separation of the field means, that the measured magnetic field is computationally divided into external and internal parts based on the field's ionospheric or telluric origin. We study the yearly directional distributions of the separated horizontal geomagnetic field and its time derivative. The yearly distributions do not have a clear solar cycle dependency. The internal field distributions are more scattered than the external field. There are also clear, station specific differences in the distributions. One of our main findings is that the direction of the geomagnetic field time derivative has a very short "reset time", around two minutes, but the total horizontal field does not have this kind of behavior. These results hold true even with less active space weather conditions. We conclude that this result gives insight into the time scale of ionospheric current systems, which are the primary driver behind the time derivative's behavior.

1 Introduction

Space weather, for example solar eruptions, can have harmful effects on Earth via *geomagnetically induced currents* (GIC). Usually GIC are weak and harmless, but due to stormy space weather they can even cause large-scale power outages. For example, in March 1989, a geomagnetic storm caused a province wide blackout in Québec, Canada (Bolduc, 2002). More thorough descriptions of space weather effects are given by, e.g., Boteler et al. (1998); Wik et al. (2009); Pulkkinen et al. (2005).

Even though the phenomenon of GIC has been studied for decades, we still do not have a complete understanding of the physics behind GIC events due to their complexity. To eventually forecast GIC events, we first need to understand the magnetic field dynamics behind them. The magnetic field that we can measure on the Earth's surface is primarily produced by *iono-*
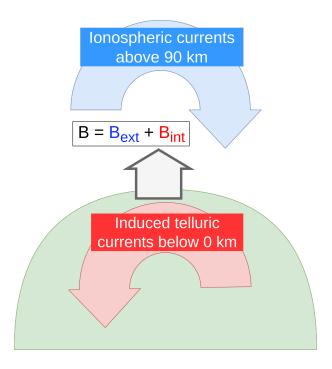
Figure 1. Represenation of the external (ionospheric), $\mathbf{B}_{ext}$, and internal (telluric), $\mathbf{B}_{int}$, components present in the measured magnetic field, $\mathbf{B}$, on Earth. Adapted from Juusola et al. (2020).

spheric and *magnetospheric currents*, and secondarily by currents induced in the conducting ground, the *telluric currents*. A representation of these external and internal sources is shown in Figure 1. We can use computational separation to divide the measured magnetic field. The separation divides the measured field into two parts; one that is created by currents in the iono-

30   sphere and magnetosphere (*external part*) and another that is created by the induced currents in the Earth's crust and mantle (*internal part*).

GIC is driven by the ground electric fields. These fields are associated with the time derivative of the geomagnetic field, $d\mathbf{B}/dt$, via Faraday's law. This is why the time derivative, $d\mathbf{B}/dt$, can be used to approximate GIC risk level (Viljanen et al., 2001). However, the behavior of the derivative is complex and has proven to be difficult to predict (Pulkkinen et al., 2011).

35   Several studies have been done focusing on $d\mathbf{B}/dt$. The study by Viljanen et al. (2001) looks at the occurrence of large values of the ground horizontal $d\mathbf{B}/dt$ on a daily, seasonal, and yearly levels and their directional distributions at IMAGE magnetometer stations in northern Europe. One of the study's findings, regarding the $d\mathbf{B}/dt$ directional distributions, is that there is no evident solar cycle dependence, but the distribution pattern is narrower in the quietest and most active years of the cycle. Viljanen and Tanskanen (2011) take a closer look on the diurnal and seasonal distributions of large $d\mathbf{B}/dt$. Among other things they find that

40   large $d\mathbf{B}/dt$ occur most commonly around local MLT midnight and early morning hours, and very rarely around midday. Also, large $d\mathbf{B}/dt$ happen mainly during westward electrojets, with southward oriented horizontal $\mathbf{B}$. One of the main findings of Pulkkinen et al. (2006) is that there is a clear change in the dynamics of magnetic field fluctuations in temporal scale from 80 to

100 seconds. They conclude that above scales of 100 s, the spatiotemporal behavior of ground horizontal $d\mathbf{B}/dt$ resembles that of uncorrelated white noise. Juusola et al. (2020) found that the internal part of the time derivative of the horizontal magnetic field ($d\mathbf{H}_{int}/dt$) is comparable to, or even larger than the external part ($d\mathbf{H}_{ext}/dt$). Their results also show that the directional distribution of $d\mathbf{H}_{int}/dt$ is much more complex than of $d\mathbf{H}_{ext}/dt$, which is explained by the 3D ground conductivity and associated telluric currents.

Our group is approaching the problem of GIC forecasting from a slightly different perspective than previous studies. Many GIC studies based on the time derivative of the ground magnetic field, e.g., Pulkkinen et al. (2006); Viljanen et al. (2001); Viljanen and Tanskanen (2011), concentrated on the total $d\mathbf{H}/dt$, which is a sum of the external and internal contribution. However, the recent study by Juusola et al. (2020) shows that actually the telluric currents dominate $d\mathbf{H}/dt$. This is the basis for our study. We use separated magnetic field measurements to find indicators for strong GIC events. Our primary interest is to deepen previous understanding of the characteristics of the magnetic field and its time derivative during active events characterized by large values of $d\mathbf{H}/dt$. In this paper, we analyze both the external and internal part of $\mathbf{H}$ and $d\mathbf{H}/dt$ and study their temporal and spatial differences.

2 Data and methods

2.1 Data

We use 10 s data from the IMAGE (International Monitor for Auroral Geomagnetic Effects) magnetometer network between 1996-2018. Locations of the IMAGE magnetometers at the beginning of 2017 are presented in Fig. 2. Quiet-time baselines are subtracted from the data using an automatic method (van de Kamp, 2013).

In this study, we use magnetic data separated into external and internal parts, as was done by Juusola et al. (2020). We use the 2D Spherical Elementary Current System method (SECS) to perform the separation. A thorough description of the SECS method is given by Vanhamäki and Juusola (2020).

2.2 Methods

The measured, baseline subtracted, horizontal magnetic field vector is given as a time series ($\mathbf{H}(t)$). Its direction is measured with respect to the (geographic) north direction positive clockwise ($\theta(t)$). We study the temporal change of θ, i.e. $\Delta\theta$, as well as the relative change in the field amplitude, $R(T)$, over a time period, T. The parameter, T, is a multiple of the 10 s time step of the time series. $\Delta\theta$ is calculated for the total variation field ($\mathbf{H} = \mathbf{H}_{tot}$), external part ($\mathbf{H}_{ext}$) and internal part ($\mathbf{H}_{int}$). In the same way, we consider the time derivative ($d\mathbf{H}/dt$) and the related direction. The relative change in the amplitude of the time derivative, is analyzed in a similar way. The main motivation behind this was to repeat a similar analysis, done in previous studies for the total field ($\mathbf{H}$), on the $\mathbf{H}_{ext}$ and $\mathbf{H}_{int}$ fields. We aim to study the differences between the external and internal magnetic field dynamics and evaluate their contribution to the GIC.
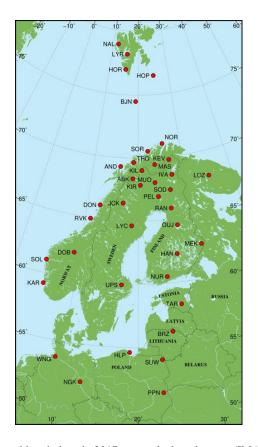
Figure 2. IMAGE station locations and name abbreviations in 2017 are marked on the map (IMAGE, 2021).

The quantaties $\mathbf{H}$, $d\mathbf{H}/dt$, θ, $\Delta\theta$, $R(T)$ and T used in this study are defined in Table 1. Our study focuses on magnetic field behavior during active space weather, characterized by large values of $|d\mathbf{H}/dt|$. For the most cases, we use a threshold value of $|d\mathbf{H}/dt| \geq 1\text{nTs}^{-1}$, where $\mathbf{H}$ is the total horizontal field. The specific questions we study are the following:

1. Is there yearly variation in directional distributions of $\mathbf{H}$ and $d\mathbf{H}/dt$?

2. How large is the geographic variability in these directional distributions and $\Delta\theta$?

3. Are there differences between the external and internal $\mathbf{H}$ and $d\mathbf{H}/dt$ in $\Delta\theta$?

4. What is the dependence of $\Delta\theta$ and $R(T)$ on T, and are there characteristic time scales?

5. Does the activity level, represented by $|d\mathbf{H}/dt|$, affect the directional and $\Delta\theta$ distribution?

We also look at the mean horizontal magnetic field directions at stations. Since we are dealing with circular data, we have to take additional measures to get a meaningful average direction. The directional distribution of the time derivative is bimodal, i.e., the values are clustered around two opposite directions (mainly north and south). The following method is used in the case of $d\mathbf{H}/dt$:

Annales
Geophysicae
Discussions

Table 1. Definitions for quantities used in this study.

Horizontal magnetic field vector	$\mathbf{H} = B_x \hat{\mathbf{e}}_x + B_y \hat{\mathbf{e}}_y$
Amplitude	$H = \sqrt{B_x^2 + B_y^2}$
Horizontal magnetic field time derivative	$d\mathbf{H}/dt = \frac{dB_x}{dt}\hat{\mathbf{e}}_x + \frac{dB_y}{dt}\hat{\mathbf{e}}_y$
Amplitude	$dH/dt = \sqrt{\frac{dB_x}{dt}^2 + \frac{dB_y}{dt}^2}$
Direction of the horizontal vector	$\theta = \arctan(\frac{B_y}{B_x})$
Change in direction (t_0 = time when $d\mathbf{H}/dt$ reaches the threshold value)	$\Delta\theta = \theta(t_0 + T) - \theta(t_0)$
Relative change in amplitude of $d\mathbf{H}/dt$	$R(T) = \frac{|dH/dt|_{t_0+T}}{|dH/dt|_{t_0}}$
Notation for the external and internal fields	$\mathbf{H}_{ext}, \mathbf{H}_{int}, d\mathbf{H}_{ext}/dt$ etc.

First we construct a histogram of eight bins of the directional values. The bins are: 1. $[0, 45)°$, 2. $[45, 90)°$, 3. $[90, 135)°$, 4. $[135, 180)°$, 5. $[180, 225)°$, 6. $[225, 270)°$, 7. $[270, 315)°$, 8. $[315, 360)°$. The second step is to find the highest bin, i.e. largest number of cases, which gives the approximate direction. (North: bins 1 and 8, East: 2 and 3, South: 4 and 5, West: 6 and 7.) The last step is to calculate the mean direction using only the values in the semicircle of the approximate direction. E.g., if the highest bin is in the east sector, calculate the mean direction using values in range 0°to 180°. For the sake of clarity, we present the mean direction in the case of the derivative in Fig. 9, for the south sector (90°to 270°) only. Meaning that, if the mean direction given by our method gave a northward direction, we add or subtract 180°.

3 Results

3.1 Example event

We first look at the magnetic field behavior during a single space weather event. Figure 3 shows magnetic field data at Tromsø (TRO, geographic latitude $= 69.66^o$ N) during one hour of the Halloween event in 2003. The panels, starting from the top, show the magnitude of the horizontal magnetic field ($\mathbf{H}$), $\mathbf{B}_x$ and $\mathbf{B}_y$ components, the magnitude of the time derivative of the field ($d\mathbf{H}/dt$), $\Delta\theta$ for $\mathbf{H}$, and $\Delta\theta$ for $d\mathbf{H}/dt$. The change in direction is calculated over $T = 1$ min. The Halloween event was one of the strongest magnetic storms on record (Pulkkinen et al., 2005; Wik et al., 2009). $d\mathbf{H}/dt$ values are large ($> 10\mathrm{nTs}^{-1}$), indicating also strong GIC. We see that there is little variation in the direction of $\mathbf{H}$ (second lowest panel), whereas its time derivative (lowest panel) has much more chaotic behavior. The $d\mathbf{H}/dt$ is changing direction very rapidly and strongly during the whole period.

3.2 Location specific differences

Next, we examine directional distributions of the separated magnetic field at the IMAGE stations. Figure 4 shows polar plots of the directional distributions of external and internal $\mathbf{H}$ at each station for one year (2017). The left panel shows $\mathbf{H}_{ext}$. We see very distinct southward distributions above latitude 64°. At lower latitudes northward direction is dominant. The distributions
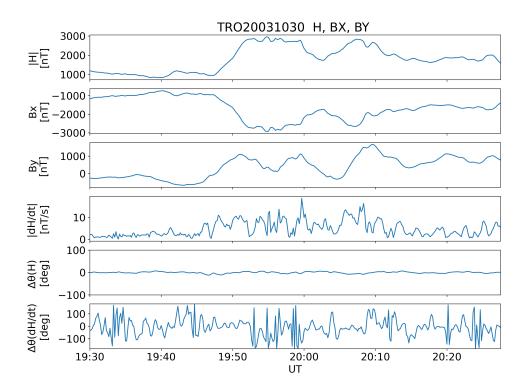
Figure 3. Horizontal magnetic field, and $\mathbf{B}_x$ and $\mathbf{B}_y$ components in Tromsø, Norway, during one hour of the Halloween event on 30th Oct 2003. Panels from the top are: 1) magnitude of the horizontal magnetic field, $\mathbf{H}$, 2) $\mathbf{B}_x$ component, 3) $\mathbf{B}_y$ component, 4) time derivative of $\mathbf{H}$, $d\mathbf{H}/dt$, 5) change in direction, $\Delta\theta(T = 1\text{ min})$ of $\mathbf{H}$, 6) $\Delta\theta(T = 1\text{ min})$ of $d\mathbf{H}/dt$.

are mostly narrow. As for $\mathbf{H}_{int}$, Fig. 4 in the right panel, there seems to be more variation in directions. The behavior of the internal field is similar to that of the external one: southward orientations above 64°N, and northward (or very scattered) distributions below that latitude.

We repeat similar analysis on the time derivative of the external and internal field (Fig. 5). Left panel shows $d\mathbf{H}_{ext}/dt$ and 110 right shows $d\mathbf{H}_{int}/dt$. The external field has, again, quite clear north-south orientations. There is a bit more scattering visible at the southern stations with less data.

As for the internal $d\mathbf{H}/dt$ there seems to be more variation between the stations. For example, Masi (MAS, geographic lat. = 69.46°N, lon. = 23.70°E) has a very clear north-east south-west orientation but in Tromsø (TRO, geographic lat. = 69.66°N, lon. = 18.94°E), the distribution looks almost even. Especially, some of the stations near the Norwegian coastline (e.g. DON, 115 RVK) seem to have very narrow distributions.

The data from stations in Germany and Poland are available, but they were not included in these plots due to very limited amount of data points fitting the criterion ($|d\mathbf{H}/dt| > 1\text{ nTs}^{-1}$). The number of data points at each station in 2017 is presented
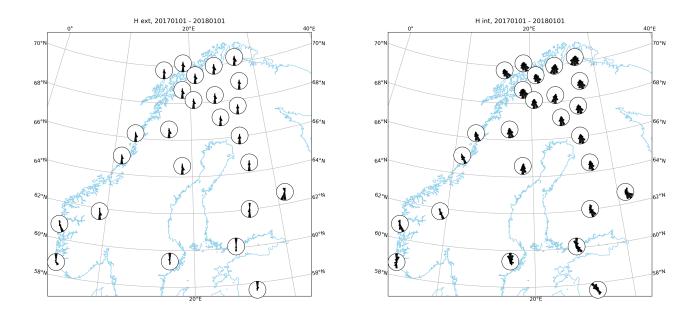
Figure 4. Directional distribution of external (left) and internal (right) $\mathbf{H}$ at IMAGE stations in 2017 when $|d\mathbf{H}/dt| > 1 \mathrm{nTs}^{-1}$.

KEV	MAS	TRO	AND	KIL	IVA	ABK	MUO	KIR	SOD
45820	59574	68884	53459	52788	47770	49274	22348	34259	32436
PEL	**JCK**	**DON**	**RAN**	**RVK**	**LYC**	**OUJ**	**MEK**	**HAN**	**DOB**
31558	26815	32876	11942	17177	14902	7624	2231	2182	2750
SOL	**NUR**	**UPS**	**KAR**	**TAR**					
1676	1259	586	425	232					

Table 2. Number of 10-s data points in 2017 fitting the criterion $|d\mathbf{H}/dt| > 1 \mathrm{nTs}^{-1}$ at each station shown on the map in Figs. 4 and 5.

in Table 2. As expected, the number of data points fitting the criterion increases towards the north. The smallest amount of data is at Tartu (TAR) (N = 232), and the highest is at Tromsø (TRO) (N = 68884).

120 **3.3 Yearly differences**

The directional distributions of $\mathbf{H}$ were also analyzed yearly, to see if the solar cycle affects these distributions, or if certain years stand out. The yearly polar plots for external and internal $\mathbf{H}$ for Sodankylä (SOD) are shown in Fig. 6. Same plots for the time derivative are shown in Fig. 7. Kevo station (KEV) shows some unexpected features that are shown in Appendix A1.
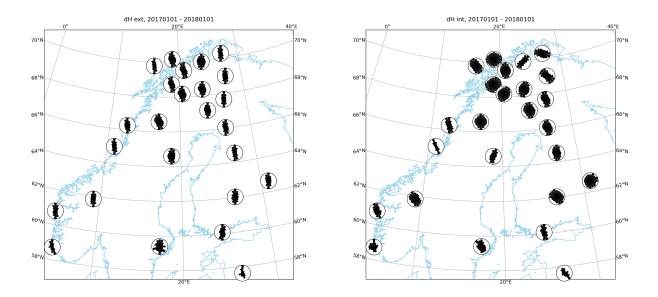
Figure 5. Directional distribution of external (left) and internal (right) $d\mathbf{H}/dt$ at IMAGE stations in 2017 when $|d\mathbf{H}/dt| > 1$ nTs^{-1}.

The external and internal $\mathbf{H}$ do not show significant variation between the years. In the plots for the external $\mathbf{H}$ (Fig. 6

125   (a)) the clear southward orientation is visible each year. External and internal $\mathbf{H}$ also show some variation in south-east and south-west directions. 1997 and 2004 seem to have equal amounts of southward and south-south-east oriented cases in external $\mathbf{H}$. As for the internal $\mathbf{H}$, the years 1997 and 2004 do not stand out compared to the other years.

Plots of the external $d\mathbf{H}/dt$ (Fig. 7 (a)) do not show any clear differences between the years. The orientations are almost strictly northward-southward. There is a bit more variation to the east and west direction in 2012 and 2013. The polar plots

130   for the time derivative of the internal $\mathbf{H}$ (Fig. 7 (b)) seems to be a bit more evenly distributed during the solar maximum years (2001, 2002 and 2012, 2013). The solar minimum years have more narrow distributions, especially 2007 and 2008.

Fig. 8 shows the diurnal distribution of events fitting the criterion for the time derivative of $\mathbf{H}$ for SOD, 1996-2018. The time is expressed in magnetic local time (MLT), and each year is shown in a separate histogram. The histograms show that every year most events take place around the magnetic midnight or early morning hours. There is a clear minimum around
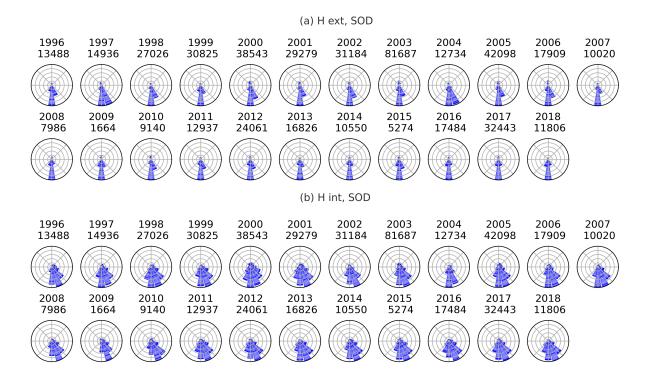
135   noon/afternoon.

Figure 6. Directional distribution of (a) $\mathbf{H}_{ext}$ and (b) $\mathbf{H}_{int}$ at Sodankylä (SOD) between 1996-2018 when $|d\mathbf{H}/dt| > 1 \, \mathrm{nTs}^{-1}$. The number of data points is plotted below the year label.

3.4 Mean directions

Fig. 9 (left panel) shows the mean directions for each year at KIL, SOD and OUJ stations for the external part (blue triangles) and internal part of (red dots) $\mathbf{H}$. The grey markers (OUJ, 2009) indicate very small amount of data, less than 100 10 s-data-points, fitting the derivative criterion that year.

140 No clear yearly trend is visible. The mean directions are strictly southward at KIL, SOD and OUJ for both external and internal parts of $\mathbf{H}$. Figure 9 (right panel) shows the mean directions for the external (blue triangles) and internal (red dots) $d\mathbf{H}_{int}/dt$. There is only little variation in the mean directions. The solar minimum year, 2009, does stand out a bit, which may be due to lack of events.

3.5 Effect of T

145 We also studied how the time, T, over which the change in $\mathbf{H}$-vector direction is considered, affects the standard deviations of $\Delta\theta$. The goal was to figure out whether it is possible to find a characteristic time scale for the magnetic field. In other words: does the standard deviation of $\Delta\theta$ of the magnetic field (or the time derivative) reach an asymptotic value as T increases? And if so, what is a typical time scale?
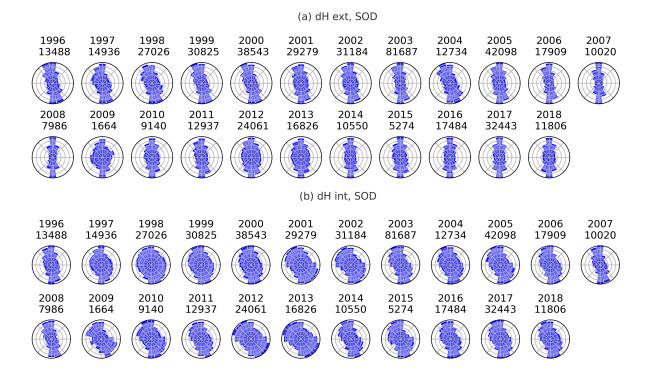
Figure 7. Directional distribution of (a) $d\mathbf{H}_{ext}/dt$ and (b) $d\mathbf{H}_{int}/dt$ at Sodankylä (SOD) 1996–2018 when $|d\mathbf{H}/dt| > 1$ nTs^{-1}. The number of data points is plotted below the year label.

Figures 10 and 11 show $\Delta\theta$ for the horizontal magnetic field and its time derivative respectively. There is a clear difference

150   in their behavior. The standard deviation of $\mathbf{H}$ is increasing faster when $T < 30$ min. After that, the increase is less steep, but there is no asymptotic value reached even after several hours. For $d\mathbf{H}/dt$, an asymptotic value is reached quickly, just after about two minutes. This behavior was seen at all the studied stations. Also considering the mean values for $\Delta\theta$ yields similar results, which are not shown here.

Figure 13 demonstrates values of the standard deviation of $\Delta\theta$ for external $d\mathbf{H}/dt$ at magnetometer stations, when $T = $

155   10 min. The values are similar at all stations ranging from 105 to 109 degrees. They all are close to the theoretical standard deviation of an even distribution, which is described in detail in the Discussion section. Examples of distribution histograms at Kiruna (KIR), for different values of T, are presented in Fig. 12. The figure shows the distributions of $\Delta\theta$ for the external $\mathbf{H}$ (left panel) and its time derivative (right panel). Starting from the top panel, we have used $T = 10$ s, $T = 30$ s, $T = 10$ min and $T = 5$ h. In the plots for the external $\mathbf{H}$, it is clearly visible how the distributions slowly even out at growing values of T.

160   Also, we see that in the lowest panel ($T = 5$ h) large values (+/- 180°) of $\Delta\theta$ become increasingly common. This means that the field is often pointing to the opposite direction after 5 hours. In the plots for the external $d\mathbf{H}/dt$, the distributions even out very quickly at larger T values. Already at $T = 30$ s the distribution for the time derivative looks quite even.
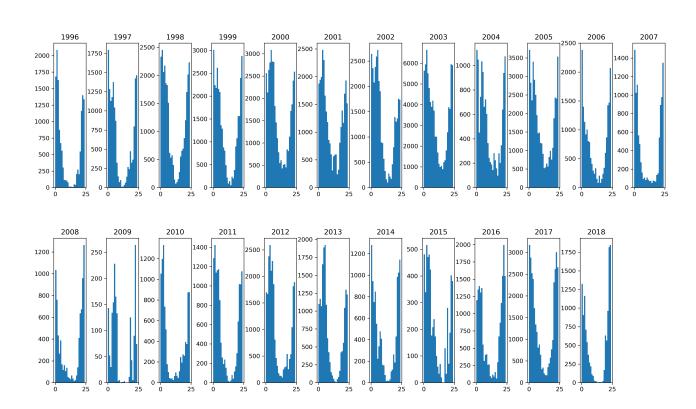
Figure 8. MLT distribution of events fitting the $d\mathbf{H}/dt >= 1$ nTs^{-1} criterion. Sodankylä (SOD), 1996–2018.

Finally we look at how the field strength changes over a period T. This is done by taking the ratio between the field amplitude at $t_0 + T$ and t_0, t_0 being the time when $d\mathbf{H}/dt$ reaches the threshold value (1 nTs^{-1}). These results are shown in Fig. 14.

165   The ratios are below 100%, meaning that the derivative field typically decreases in amplitude after reaching the limit value (1 nTs^{-1}). The standard deviation is the smallest at the shortest time period, $T = 10$ s.

3.6   Effect of $d\mathbf{H}/dt$ activity level

Effect of a smaller threshold value for the time derivative was also studied. The other threshold that we used is 0.5 nTs^{-1} < $d\mathbf{H}/dt$ < 1 nTs^{-1}. Figure B2 in Appendix shows the standard deviations of $\Delta\theta$ at different values of T, using smaller threshold.

170   Overall, we get very similar results for these less active cases (i.e. similar asymptotic value) in the study of $\Delta\theta$.
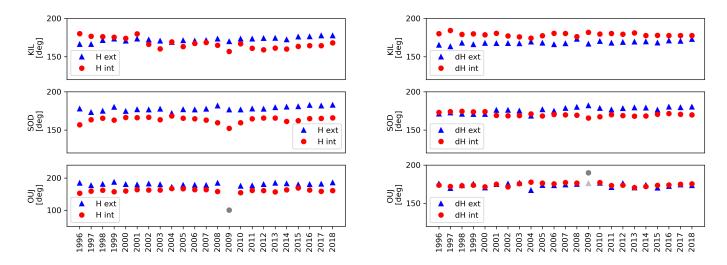
Figure 9. Mean directions of external and internal $\mathbf{H}$ (left panel) and $d\mathbf{H}/dt$ (right panel) as a function of year at KIL, SOD and OUJ, 1996-2018. $\mathbf{H}_{ext}$ is marked with blue triangles and $\mathbf{H}_{int}$ with red dots. The grey markers indicate very few events (less than 100) fitting the criterion that year.
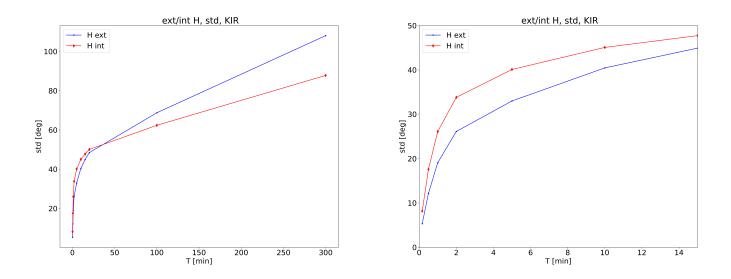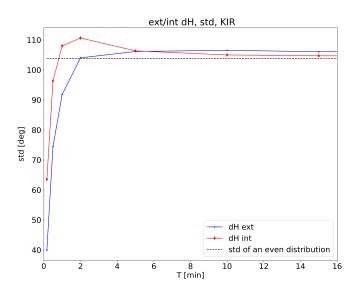

Figure 10. Standard deviations of $\Delta\theta$ for the external (blue line with dot markers) and internal (red line with diamond markers) $\mathbf{H}$ as a function of T at Kiruna (KIR). Threshold value for chosen events is $|d\mathbf{H}/dt| > 1 \, \mathrm{nTs}^{-1}$. On the left, T range is from 0 to 300 min, a closeup on the first 15 min is shown on the right.

Figure 11. Standard deviations of $\Delta\theta$ for the external (blue line with dot markers) and internal (red line with diamond markers) $d\mathbf{H}/dt$ as a function of T at Kiruna (KIR). Threshold value for chosen events is $|d\mathbf{H}/dt| > 1 \text{ nTs}^{-1}$.

4 Discussion

4.1 Magnetic field separation

In this analysis we studied the directional distributions and change in the direction of the separated horizontal magnetic field and its time derivative. The separation was done to better understand the dynamics behind large GIC events. Previous studies

175 have shown that $d\mathbf{B}/dt$ is a good indicator for GIC. Separating the field makes it possible to study individual contributions of the external and internal fields.

The separation of the geomagnetic field can be done using several different methods, and each of them has their own advantages and disadvantages (e.g., Holschneider et al., 2016). The separation of the fields is never fully accurate, and there will be a small portion of external field present in the internal field, and vice versa. The effect of using the 2D SECS method

180 for the separation should be considered. It is possible that some of the effects seen in this analysis, could be produced by the method. This could be verified in future studies, by repeating this analysis using a different method for the field separation. Also, the number and density of magnetometer stations has changed over the studied period, which may also affect the accuracy of the field separation.
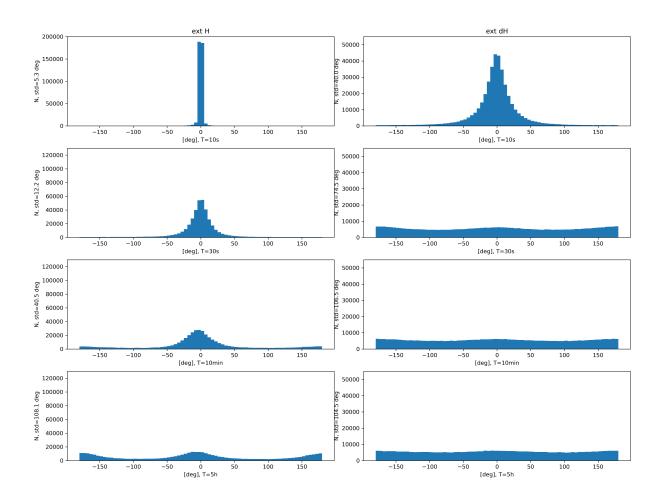
Figure 12. Examples of $\Delta\theta$ distributions of external **H** (left panel) and external $d\mathbf{H}/dt$ (right panel) at Kiruna (KIR) with different values of T. From top to bottom: $T = 10$ sec, 30 sec, 10 min and 5 hours. The distributions even out at greater T values.

4.2 Directional distributions

185   The dominant north-south orientation of the directional distributions is caused by the eastward and westward electrojets. The westward electrojet produces southward magnetic field, and this occurs after the magnetic midnight. Majority of the events chosen with the derivative criterion happen during these times, as is seen in the time distributions in Fig. 8. This is not a new result, and has been described in previous studies. For example, Viljanen et al. (2001) had very similar results regarding the directional distribution of $d\mathbf{H}/dt$: mainly southward **H** field, with $d\mathbf{H}/dt > 1$ nTs^{-1}, and a lot more scattered directional

190   distributions for the time derivative.

    We also noticed clear differences between magnetometer stations located at similar latitudes with $d\mathbf{H}_{int}/dt$. The station specific differences with directional distributions near the Norwegian coastline (e.g. DON, RVK) are likely due to the local
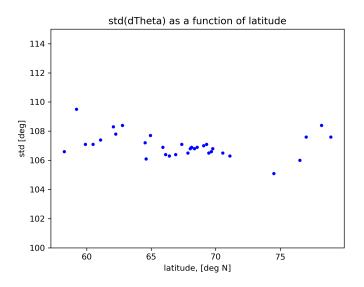
Figure 13. Standard deviation of $\Delta\theta$ for external $d\mathbf{H}/dt$ at IMAGE stations as a function of latitude. Data from 1996 to 2018, and $T = 10$ min.
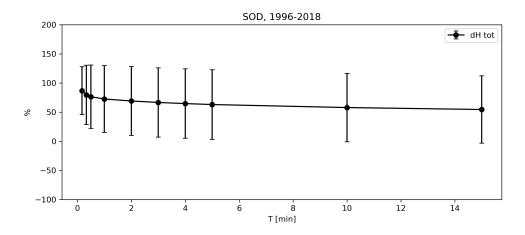

Figure 14. Mean values and standard deviation of R(T) (relative change in amplitude) for total $d\mathbf{H}/dt$ at SOD. Data from 1996 to 2018, and $T = 10$ s ... 15 min.

conductivity differences caused by the highly conducting seawater, also known as *the coast effect* (Lilley, 2007). However, e.g. Masi (MAS), which is located inland, also has a narrow distribution, which is known to be due to highly conducting, near-surface structures that strongly affect the geomagnetic field (Viljanen et al., 1995).

15

4.2.1 Mean directions

Defining the yearly mean direction in case of $\mathbf{H}$ is straightforward. However, with the time derivative, we get a lot more scattered distributions, for which getting a meaningful mean direction requires some additional steps. The method we used is a simple way to get an approximate mean direction for a circular distribution. We also tried a few other methods (e.g. by Davis

200 (2002)) for getting the mean direction, but they proved to be somewhat impractical with very scattered distributions.

4.3 Effect of T

The behavior of the $\mathbf{H}$ and $d\mathbf{H}/dt$ vectors differ greatly from each other. One of the main, new discoveries in this research, was the asymptotic value and characteristic time scale of the derivative vector. The asymptotic values of the standard deviations of $\Delta\theta$ for external and internal $d\mathbf{H}/dt$, can be explained via the value distributions and theoretical value for a uniform distribution.

205 Standard deviation, σ, for the uniform distribution between values a and b, is given by equation 1. This is easily proven with basic equations for variance and probability density of a uniform distribution (Bertsekas and Tsitsiklis, 2008). In our study, where the magnetic field direction values range from a = -180 to b = 180 degrees, this theoretical value is approximately 104°:

$$\sigma = \frac{b-a}{\sqrt{12}} = \frac{360}{\sqrt{12}} \approx 103.9 \qquad (1)$$

This value is close to the asymptotic values we got for the $\Delta\theta$ of $d\mathbf{H}/dt$, ranging from 104 to 110 for the studied stations.

210 Values significantly above 104°, as is the case for large T values for $\Delta\theta$ of $\mathbf{H}$, indicate that the distribution is not uniform. This is evident in Fig. 12, where the $\Delta\theta$ distribution of $\mathbf{H}$ at $T = 5$ h shows two peaks, one around 0° and another around +/- 180°. The distribution of the derivative is visibly more even. However, when using longer periods of T, we end up comparing entirely different events affected by different ionospheric current systems. This raises the question if it even makes sense to use such long periods for T.

215 Our analysis and that of Pulkkinen et al. (2006) both yield, through different methods, the same 80 s to 100 s time scale for the behavior of $d\mathbf{H}/dt$. After this time, the behavior of $d\mathbf{H}/dt$ resembles that of white noise, i.e., any memory of the past is lost. It is not clear, though, why the critical time is just 80–100 s. The size, motion, and lifetime of the $d\mathbf{H}/dt$ structures may contribute to the observed time scale. Because of the highly variable ground conductivity, development of the external $d\mathbf{H}/dt$ structures is generally much smoother than that of the internal $d\mathbf{H}/dt$ structures (Juusola et al., 2020). This can also be seen in

220 Fig. 11, where the standard deviation of $\Delta\theta$ for the internal $d\mathbf{H}/dt$ is clearly higher than that for the external $d\mathbf{H}/dt$ during the first few minutes.

Also Belakhovsky et al. (2018) studied the directional variation of the horizontal magnetic field and its derivative. They used a so-called *RB parameter* to determine if the field is changing more in magnitude or in direction. This parameter is similar to the $\Delta\theta$ quantity used in our study. For example, in a 2D-case, $\mathbf{B}(t) = \{X, Y\}$ and length of time series N, the RB-parameter

225 is given by (Du et al., 2005)

$$RB = 1 - \frac{1}{N}\sqrt{\left(\sum_{n=1}^{N}\cos_x\alpha\right)^2 + \left(\sum_{n=1}^{N}\cos_y\alpha\right)^2} \qquad (2)$$

where the magnitude of magnetic disturbance is $|\Delta B| = \sqrt{\Delta X^2 + \Delta Y^2}$, and the directions $\cos_x \alpha = \Delta X/|\Delta B|$ and $\cos_y \alpha = \Delta Y/|\Delta B|$. They used the total variation field, and not the separated field like we do. Consistently with our study they discovered that the directional variability of $d\mathbf{B}/dt$ is greater than that of the variation field, $\mathbf{B}$. This was explained by the small-scale currents structures, the non-stationary vortex structures created by the local field-aligned currents.

In addition to the change in direction, we also looked at how the amplitude of total $d\mathbf{H}/dt$ changes over the time period, T (Fig. 14). The relative change in amplitude, R(T), was below 100% at all studied values of T, meaning that the amplitude of the derivative tends to decrease immediately after reaching the threshold value. The mean value for R(T) is the highest at $T = 10$ s. This is reasonable since the derivative changes very rapidly, e.g. the case study in Fig. 3. It is rare for the derivative amplitude to remain at high values for long periods. The standard deviation slightly increases when T increases, meaning that variation in the amplitude is smallest immediately after the amplitude reaches the threshold value.

4.4 Effect of activity level

In the last part of our study we tested a smaller threshold value for the horizontal time derivative. This smaller limit seems to have no major impact on the main results, i.e. the characteristic time scale of the derivative vector, or the relative change in amplitude. Plots, using the smaller threshold value, for the standard deviation of $\Delta\theta$ are presented in Appendix B1, B2, and for R(T) in Appendix B3. This result implies that the characteristic time scale is not related only to the most active events, but is visible also during the less active periods.

4.5 Forecasting GIC

Forecast of $d\mathbf{H}/dt$ would require two things: prediction of the external $d\mathbf{H}/dt$ from observed solar wind driving of the Earth's magnetosphere and ionosphere and prediction of the induction in the conducting ground as driven by the dynamics of the ionospheric and magnetospheric current systems. The latter part is relatively well understood [e.g., Ivannikova et al. (2018); Marshalko et al. (2021)] and mainly hampered by insufficiently detailed models of the Earth's conductivity. The first part is still a challenge, but hopefully global simulations will at some point be able to provide this. A few time steps forward the development of the external $d\mathbf{H}/dt$ could maybe be predicted by observing the dynamics of the $d\mathbf{H}/dt$ structures, e.g. Apatenkov et al. (2020). Behavior of the ground magnetic field vector differs markedly from that of its time derivative. Most likely this is not a unique feature of the geomagnetic field but applies more widely to various vector quantities such as the solar wind and the atmospheric wind on the Earth's surface. Similar analysis of the interplanetary magnetic field, for instance, might yield some insights on the structure of the field.

5 Conclusions

In this study we first looked at directional distributions of $\mathbf{H}$ and $d\mathbf{H}/dt$ separately for the external and internal magnetic fields. We discovered:

1. Mainly southward orientations with $\mathbf{H}$, and north-south orientations with $d\mathbf{H}/dt$. This also backs up results from previous research (e.g. Viljanen and Tanskanen (2011)).

2. Clear, station specific differences in the directional distribution of $d\mathbf{H}_{int}/dt$. These may be due to ground conductivity differences at the respective stations. Also the coastal effect is visible in the results.

3. There is little variation in the directional distributions and mean directions between different years. However, $d\mathbf{H}_{int}/dt$ has more scattered distributions than $d\mathbf{H}_{ext}/dt$.

In the last part of our analysis we studied the directional change of $\mathbf{H}$ over varying time periods, T, $\Delta\theta$, and its standard deviation. The main new result discovered in this analysis is the asymptotic value, of about 104-110°, for $d\mathbf{H}/dt$ standard deviation. This was reached at about $T = 2$ min. We understand this so that the time derivative's direction is not predictable based on the previous values. In other words, the time derivative of the geomagnetic field quickly "loses" its memory.

Code and data availability. IMAGE data used in this study is available at the website: https://space.fmi.fi/image (IMAGE, 2021). The code used to calculate magnetic local times is available at https://apexpy.readthedocs.io/en/latest/ (van der Meeren and Burrell, 2015)

Annales
Geophysicae
Discussions
EGU
Open Access

Appendix A: Yearly distributions, Kevo (KEV)

270　During this analysis we also discovered a curious feature in Kevo (KEV) internal $d\mathbf{H}/dt$ directional distribution, presented
in Fig. A1. The distribution of the internal $d\mathbf{H}/dt$ rotates towards the east-west orientation in 2009 and stays like that until
2018. 2009 is one of the solar minimum years. There are significantly fewer data points that years. Amount of data drops
from around 20000 to about 4000. However, the east-west orientation is visible even during the next solar maximum. The
investigation for the reason behind this is still under way. Our best guess is that the tilt in the distribution could have been
275　caused by the installation of a new device, or e.g. power cables, on the KEV research station in the beginning of 2009. More
specifically, this happened in January or February 2009, as can be seen in Fig. A2. For this monthly plot we used a smaller
threshold ($d\mathbf{H}/dt > 0.5$ nTs^{-1}) to get more data points.

Appendix B: Effect of the activity level

We also tested a smaller threshold value for the time derivative, 0.5 nTs$^{-1} < |d\mathbf{H}/dt| < 1$ nTs^{-1}. In this section we repeat
280　the analysis for the change in $\mathbf{H}$ and $d\mathbf{H}/dt$ direction, $\Delta\theta$ (Fig. B1), its standard deviation (Fig. B2) and relative change in
amplitude, $R(T)$ (Fig. B3). There is no notable difference compared to the graphs made using the higher threshold.
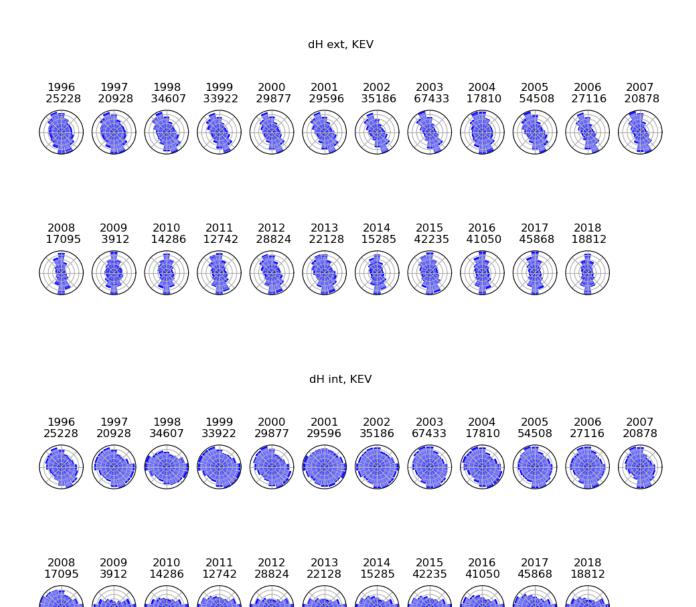
Figure A1. Yearly directional distributions of $d\mathbf{H}/dt$ at Kevo (KEV), 1996-2008. Upper panel: external $d\mathbf{H}/dt$, lower panel: internal $d\mathbf{H}/dt$. The number of data points is plotted under the year label.
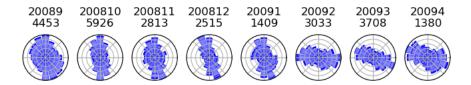
Figure A2. Monthly directional distributions of internal $d\mathbf{H}/dt$ at Kevo (KEV), 2008-09 to 2009-04. The number of data points is plotted under the year and month label. $|d\mathbf{H}/dt| > 0.5 \text{ nTs}^{-1}$.
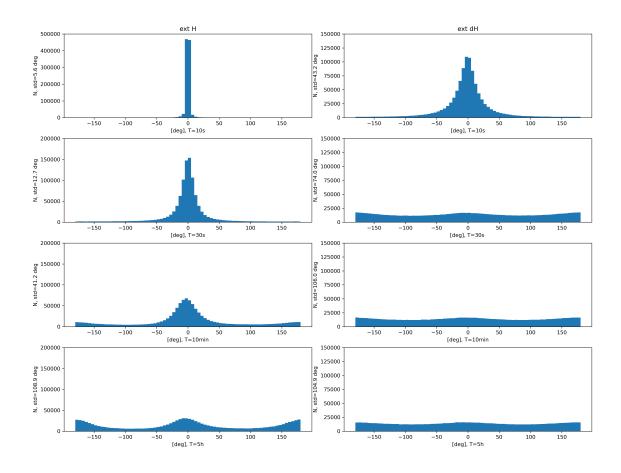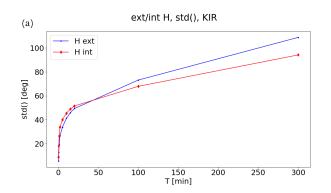

Figure B1. Histograms of $\Delta\theta$ at KIR at different time periods, T, using a threshold value $0.5 \text{ nTs}^{-1} < |d\mathbf{H}/dt| < 1 \text{ nTs}^{-1}$. On left: external $\mathbf{H}$, on right: external $d\mathbf{H}/dt$.

Figure B2. Standard deviation of $\Delta\theta$ at different time periods, T, using a threshold value $0.5 \text{ nTs}^{-1} < |d\mathbf{H}/dt| < 1 \text{ nTs}^{-1}$. Figure (a) external and internal $\mathbf{H}$, (b) external and internal $d\mathbf{H}/dt$.
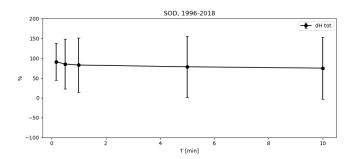

Figure B3. Mean values and standard deviation of R(T) (relative change in amplitude) for total $d\mathbf{H}/dt$ at SOD. Data from 1996 to 2018, and $T = 10$ s ... 10 min.

Annales
Geophysicae
Discussions

Author contributions. MK prepared most of the material and wrote the text with contributions from AV and LJ. SK provided help and ideas with data analysis and interpreting the results. AV and LJ provided expertise on the theoretical discussion.

Competing interests. The authors declare that they have no competing interests.

References

Apatenkov, S. V., Pilipenko, V. A., Gordeev, E. I., Viljanen, A., Juusola, L., Belakhovsky, V. B., Sakharov, Y. A., and Selivanov, V. N.: Auroral Omega Bands are a Significant Cause of Large Geomagnetically Induced Currents, Geophysical Research Letters, 47, https://doi.org/10.1029/2019GL086677, 2020.

295 Belakhovsky, V. B., Pilipenko, V. A., Sakharov, Y. A., and Selivanov, V. N.: Characteristics of the variability of a geomagnetic field for studying the impact of the magnetic storms and substorms on electrical energy systems, Izvestiya, Physics of the Solid Earth, 54, 52–65, https://doi.org/10.1134/S1069351318010032, 2018.

Bertsekas, D. P. and Tsitsiklis, J. N.: Introduction to probability, pp. 145–146, Optimization and computation series, Athena scientific, 2nd ed edn., 2008.

300 Bolduc, L.: GIC observations and studies in the Hydro-Québec power system, Journal of Atmospheric and Solar-Terrestrial Physics, 64, 1793–1802, 2002.

Boteler, D., Pirjola, R., and Nevanlinna, H.: The effects of geomagnetic disturbances on electrical systems at the Earth's surface, Advances in Space Research, 22, 17–27, https://doi.org/10.1016/S0273-1177(97)01096-X, 1998.

Davis, J. C.: Statistics and data analysis in geology, Wiley, New York, 3rd ed. edn., 2002.

305 Du, J., Wang, C., Zhang, X., Shevyre, N., and Zastenker, G.: Magnetic Field Fluctuations in the Solar Wind, Foreshock and Magnetosheath: Cluster Data Analysis, Chinese Journal of Space Science, 25, 368, https://doi.org/10.11728/cjss2005.05.368, 2005.

Holschneider, M., Lesur, V., Mauerberger, S., and Baerenzung, J.: Correlation-based modeling and separation of geomagnetic field components, Journal of Geophysical Research: Solid Earth, 121, 3142–3160, https://doi.org/10.1002/2015JB012629, _eprint: https://onlinelibrary.wiley.com/doi/pdf/10.1002/2015JB012629, 2016.

310 IMAGE: IMAGE-International Monitor for Auroral Geomagnetic Effects, https://space.fmi.fi/image/, accessed: 2021-11-25, 2021.

Ivannikova, E., Kruglyakov, M., Kuvshinov, A., Rastätter, L., and Pulkkinen, A.: Regional 3-D Modeling of Ground Electromagnetic Field Due To Realistic Geomagnetic Disturbances, Space Weather, 16, 476–500, https://doi.org/10.1002/2017SW001793, _eprint: https://onlinelibrary.wiley.com/doi/pdf/10.1002/2017SW001793, 2018.

Juusola, L., Vanhamäki, H., Viljanen, A., and Smirnov, M.: Induced currents due to 3D ground conductivity play a major role in the inter-
315 pretation of geomagnetic variations, Annales Geophysicae, 38, 983–998, https://doi.org/10.5194/angeo-38-983-2020, 2020.

Lilley, T.: COAST EFFECT OF INDUCED CURRENTS, in: Encyclopedia of Geomagnetism and Paleomagnetism, edited by Gubbins, D. and Herrero-Bervera, E., pp. 61–65, Springer Netherlands, Dordrecht, https://doi.org/10.1007/978-1-4020-4423-6_27, 2007.

Marshalko, E., Kruglyakov, M., Kuvshinov, A., Juusola, L., Kwagala, N. K., Sokolova, E., and Pilipenko, V.: Comparing Three Approaches to the Inducing Source Setting for the Ground Electromagnetic Field Modeling due to Space Weather Events, Space Weather,
320 19, e2020SW002 657, https://doi.org/10.1029/2020SW002657, _eprint: https://onlinelibrary.wiley.com/doi/pdf/10.1029/2020SW002657, 2021.

Pulkkinen, A., Lindahl, S., Viljanen, A., and Pirjola, R.: Geomagnetic storm of 29-31 October 2003: Geomagnetically induced currents and their relation to problems in the Swedish high-voltage power transmission system: GEOMAGNETICALLY INDUCED CURRENTS, Space Weather, 3, n/a–n/a, https://doi.org/10.1029/2004SW000123, 2005.

325 Pulkkinen, A., Klimas, A., Vassiliadis, D., Uritsky, V., and Tanskanen, E.: Spatiotemporal scaling properties of the ground geomagnetic field variations, Journal of Geophysical Research, 111, A03 305, https://doi.org/10.1029/2005JA011294, 2006.

Pulkkinen, A., Kuznetsova, M., Ridley, A., Raeder, J., Vapirev, A., Weimer, D., Weigel, R. S., Wiltberger, M., Millward, G., Rastätter, L., Hesse, M., Singer, H. J., and Chulaki, A.: Geospace Environment Modeling 2008–2009 Challenge: Ground magnetic field perturbations, Space Weather, 9, https://doi.org/10.1029/2010SW000600, _eprint: https://onlinelibrary.wiley.com/doi/pdf/10.1029/2010SW000600, 2011.

van de Kamp, M.: Harmonic quiet-day curves as magnetometer baselines for ionospheric current analyses, Geoscientific Instrumentation, Methods and Data Systems, 2, 289–304, https://doi.org/10.5194/gi-2-289-2013, 2013.

van der Meeren, C. and Burrell, A. G.: Contents — Apex Python library "1.1.0" documentation, https://apexpy.readthedocs.io/en/latest/, 2015.

Vanhamäki, H. and Juusola, L.: Introduction to Spherical Elementary Current Systems, in: Ionospheric Multi-Spacecraft Analysis Tools: Approaches for Deriving Ionospheric Parameters, edited by Dunlop, M. W. and Lühr, H., pp. 5–33, Springer International Publishing, https://doi.org/doi:10.1007/978-3-030-26732-2_2, 2020.

Viljanen, A. and Tanskanen, E.: Climatology of rapid geomagnetic variations at high latitudes over two solar cycles, Annales Geophysicae, 29, 1783–1792, https://doi.org/10.5194/angeo-29-1783-2011, 2011.

Viljanen, A., Kauristie, K., and Pajunpää, K.: On induction effects at EISCAT and IMAGE magnetometer stations, Geophysical Journal International, 121, 893–906, https://doi.org/10.1111/j.1365-246X.1995.tb06446.x, 1995.

Viljanen, A., Nevanlinna, H., Pajunpää, K., and Pulkkinen, A.: Time derivative of the horizontal geomagnetic field as an activity indicator, Annales Geophysicae, 19, 1107–1118, https://doi.org/10.5194/angeo-19-1107-2001, 2001.

Wik, M., Pirjola, R., Lundstedt, H., Viljanen, A., Wintoft, P., and Pulkkinen, A.: Space weather events in July 1982 and October 2003 and the effects of geomagnetically induced currents on Swedish technical systems, Annales Geophysicae, 27, 1775–1787, https://doi.org/10.5194/angeo-27-1775-2009, 2009.